
01 Jun 2017

Raman Spectral Variation for Human Fingernails of Postmenopausal Women is Dependent on Fracture Risk and Osteoporosis Status

J. R. Beattie


M. C. Caraher

N. M. Cummins

O. M. O'Driscoll

et. al. For a complete list of authors, see https://scholarsmine.mst.edu/che_bioeng_facwork/1100

Follow this and additional works at: https://scholarsmine.mst.edu/che_bioeng_facwork

 Part of the [Biochemical and Biomolecular Engineering Commons](#), and the [Biomedical Devices and Instrumentation Commons](#)

Recommended Citation

J. R. Beattie et al., "Raman Spectral Variation for Human Fingernails of Postmenopausal Women is Dependent on Fracture Risk and Osteoporosis Status," *Journal of Raman Spectroscopy*, vol. 48, no. 6, pp. 813 - 821, Wiley, Jun 2017.

The definitive version is available at <https://doi.org/10.1002/jrs.5123>

This Article - Journal is brought to you for free and open access by Scholars' Mine. It has been accepted for inclusion in Chemical and Biochemical Engineering Faculty Research & Creative Works by an authorized administrator of Scholars' Mine. This work is protected by U. S. Copyright Law. Unauthorized use including reproduction for redistribution requires the permission of the copyright holder. For more information, please contact scholarsmine@mst.edu.

AIRsight

Infrared/Raman Microscope



Raman and FTIR Microscopy in Perfect Harmony

Shimadzu's one-of-a-kind AIRsight™ Infrared/Raman Microscope delivers more accurate results and improves operational efficiency by providing complementary molecular information in one space-saving platform.

- ▶ Significantly improves the accuracy of qualitative analysis by enabling both infrared and Raman measurements from the same position without moving the sample
- ▶ Improves sample observation efficiency with proprietary wide-view camera and microscope camera for infrared measurements and objective lens for Raman measurements
- ▶ Easier operation with smart software that easily switches between infrared and Raman measurements via the same window
- ▶ Combined system saves valuable bench space

Learn more about Shimadzu's AIRsight. Call (800) 477-1227 or visit us online at

www.ssi.shimadzu.com

Shimadzu Scientific Instruments Inc., 7102 Riverwood Dr., Columbia, MD 21046, USA



Raman spectral variation for human fingernails of postmenopausal women is dependent on fracture risk and osteoporosis status

J. R. Beattie,^{a*} M. C. Caraher,^b N. M. Cummins,^c O. M. O'Driscoll,^d R. Eastell,^e S. H. Ralston^f and M. R. Towler^{g,h}

Patients diagnosed with osteoporosis have reported loss of fingernail resilience as the disease progresses. Keratin is the predominant protein in human nail tissue, and its structure has been postulated to be different in fingernails clipped from subjects who have sustained fragility fractures and those who have not, which may offer a window into the donor's bone health. This study was designed to qualify these differences, which may lead to the development of a novel screening tool for fracture risk. Raman spectroscopy was used to measure the fingernails of 633 postmenopausal women who presented at six fracture clinics located across the UK and Ireland. The Raman signals from donor's fingernails were compared between (1) fracture and nonfracture and (2) osteoporotic versus non-osteoporotic donors. The data presented show differences in the protein changes observed for pervasive osteoporosis compared to a general increased risk of fragility fracture. For fracture risk, compositional changes falling into broad classes of amino acid residue (aliphatic, aromatic, acidic, amide and sulphurous) were observed, while a difference in disulphide bonding levels was reaffirmed. For pervasive osteoporosis, the disulphide mode suggested increasing disorder in disulphide bonding orientation. Fractures were associated with a transition from alpha helical secondary structure to random, while the pervasive osteoporosis cases were associated with a transition to beta sheet structure. General fracture risk is associated with a change in the structure and composition of the keratin protein. Osteoporosis is associated with different protein structural changes and an increase in free acid groups. Copyright © 2017 John Wiley & Sons, Ltd.

Keywords: keratin; bone health; fracture risk; osteoporosis; protein

Introduction

The current reference standard for the diagnosis of osteoporosis and assessment of fracture risk is measurement of bone mineral density (BMD) using dual energy X-ray absorptiometry (DXA). In the developed world, the lifetime risk of a fracture in Caucasian women is between 30 and 40%.^[1] Responding to the rising population burden of the disease, the World Health Organization (WHO) has identified a need for improved prognostic indicators and alternatives to BMD-based diagnostic tools to assess fracture risk.^[2–5]

Anecdotally, patients diagnosed with osteoporosis have reported loss of fingernail resilience with disease progression.^[6] Preliminary studies carried out by the authors have identified a link between the Raman spectra of human nail and both osteoporosis and fracture risk of the participant.^[7–9] The authors hypothesized that this link was due to the sensitivity of Raman spectroscopy in identifying differences in protein structure, thus facilitating the use of nail protein structure as a surrogate marker for bone protein structure. Keratin and type I collagen are the two key proteins in nail and bone, respectively^[7]; they both undergo post-translational modifications and exhibit the same major characteristic peaks in key regions of Raman spectra.^[10,11]

A number of studies have investigated the use of Raman spectroscopy for probing nail composition and structure, including analysing hydration levels,^[12] comparing finger and toe nails,^[13] comparing the structure and composition of keratins in nail and other tissues^[14] and analysing nails and claws from different species.^[15] Widaja and Garland used band target entropy

minimization to separate out the signals that contribute to the Raman spectra of human nail, identifying a range of amino acid signals alongside factors that were explained as arising from protein structure,^[16] and Mussato *et al.* explored the relationship between the Raman spectra of human nail and the BMD of the

* Correspondence to: J. Renwick Beattie, Exploristics Ltd, Floor 4, 24 Linenhall Street, Belfast BT2 8BG, UK.

E-mail: rene.beattie@exploristics.com; rene@jrenwickbeattie.com

a Exploristics Ltd, Floor 4, 24 Linenhall Street, Belfast BT2 8BG, UK

b ICON plc, South County Business Park, Leopardstown, Dublin, Ireland

c Centre for Interventions in Infection, Inflammation and Immunity, Graduate Entry Medical School, University of Limerick, Limerick, Ireland

d Medical Engineering Design and Innovation Centre, Cork Institute of Technology, Cork, Ireland

e Academic Unit of Bone Metabolism, Metabolic Bone Centre, Northern General Hospital, Sheffield, UK

f School of Molecular and Clinical Medicine, Western General Hospital, Edinburgh, UK

g Department of Biomedical Engineering, Faculty of Engineering, University of Malaya, Kuala Lumpur, Malaysia

h Department of Mechanical and Industrial Engineering, Ryerson University, Toronto, Canada

donor, although the limited data processing methods that they employed prevented the identification of significant association.^[17]

The research contained herein further investigates the link between the Raman spectra of the human nail and the underlying bone health of the donor with the aim of qualifying the biochemical changes observed. This was achieved by investigating the Raman signature of the chemical bonds in fingernail keratin that are distinct between those who have good bone health and those who have not. Two separate aspects of bone health are compared, fracture and osteoporosis (osteoporosis is present in approximately 30–40% of fragility fractures). Clinical aspects of the study are reported in Beattie *et al.*^[18]

Materials and methods

Study design and patient population

A clinical study entitled 'Fracture Risk Assessment by Nail correlation study' was designed to test the link between nail keratin and the current status of bone health of the nail donors. This was a cross-sectional, international, multi-centre study designed to determine the sensitivity and specificity of Raman spectroscopy for assessment of fracture risk. Two distinct gold standard measurements of bone health were recorded for each patient: fracture history and BMD, assessed using DXA. Sample collection was carried out at six centres with ethical approval obtained at each site, and the research followed the tenets of the Declaration of Helsinki.^[19] The centres were Southampton University Hospitals NHS Trust (Southampton, England, UK), Western General Hospital Edinburgh (Edinburgh, Scotland, UK), Sheffield Teaching Hospitals NHS Foundation Trust (Sheffield, England, UK), Cardiff University Academic Centre Llandough Hospital (Cardiff, Wales, UK), Greater Glasgow and Clyde NHS Trust (Glasgow, Scotland, UK) and the Mid-Western Regional Hospital Limerick (Limerick, Ireland), providing a wide geographical distribution in terms of the British Isles. Informed consent was obtained from all recruits to the study, and all samples and records were anonymized. A total of 633 eligible women were recruited in this study. Samples from four of the centres were used for calibration with the samples from the remaining two reserved for validation of the procedures and algorithms.

Active Caucasian females aged between 50 and 85 years (inclusive) who were at least 5 years postmenopause and who presented for a DXA scan at each participating centre were invited to enrol. The subjects were required to have at least 2 mm of clippable nail. Exclusions were made based on any diseases or medication known to affect bone health. Any fractures with a traumatic cause (e.g. road traffic collision) were excluded. Sample analysis and data analysis protocols were altered from the originally proposed protocol for the study following identification of high sources of sampling variance in the original sampling procedure.

Sample analysis

Nail clippings were placed in a 1.5-ml microtube tube labelled with a unique identifier code that allowed identification of the collection centre but anonymized the patient. The samples were stored at room temperature and shipped to a central laboratory at the University of Limerick. Final sample analysis was carried out at the Clinical Translational Research and Innovation Centre (Londonderry, UK). A clinical health questionnaire was also completed which included questions pertinent to bone health. Subjects underwent DXA scans following WHO guidelines, and

the BMD data recorded were converted into DXA T-scores according to the specifications of the individual manufacturer/model of each scanner used. Subjects were not required to return to the clinic for follow-up procedures pertaining to this study, and aside from the DXA and collection of nail samples, no additional procedures were performed.

Raman spectroscopy

The Raman spectra were recorded by a Sierra Reader (Snowy Range Instruments, Laramie, WY, USA) using 785-nm excitation with 50-mW power at the sample, with the laser rastered over a 2-mm-diameter area. Three measurements per sample were recorded at spatially distinct areas of each nail, with a measurement time of 1 min. The analyst was blinded to the identity and history of the samples. Spectra were saved as tab delimited ASCII files.

Sample grouping

The samples collected in the study were divided into groups for the purpose of classification and comparison, comparing fracture *versus* nonfracture and comparing osteoporotic *versus* non-osteoporotic.

For the fracture-based comparison, the groups were as follows:

Nonfracture (control) group: Women with no history of fracture after the age of 18 years.

Fracture case group: Women with a history of fracture over the age of 45 years (excluding major trauma, e.g. car crash)

For the osteoporosis comparison, the groups were as follows:

Normal (control): DXA *t*-score > -1

Osteoporotic: DXA *t*-score ≤ -2.5

In this study, only samples meeting the DXA score criteria at all three sites (femoral neck, wrist and vertebrae) measured were included in the respective group, to create a set of samples from participants with pervasive osteoporosis (standard osteoporosis definition as recommended by the WHO^[20] is that only one out of three sites needs to meet this threshold). Previous studies have suggested that the Raman changes to nails due to osteoporosis are subtle,^[6–9] so a more extreme set of criteria was applied to enhance the contrast between the two groups. Throughout the paper, 'healthy' is used to describe samples that were classified as 'normal' through DXA assessment, unless clarified otherwise or if used in a context unrelated to discussing samples.

All data analysis was performed in Matlab 2013a (Mathworks, Cambridge, UK). Data collected from four of the centres (representing 75% of total participant number) were combined and used as a training set to calibrate the required data processing and analysis algorithms. The fracture status of the samples within the calibration set was un-blinded at this stage to allow calibration against the relevant parameters. All data processing procedures and data analysis algorithms remained blinded to the data from the remaining two centres at this stage, and only the calibration set was used to optimize these steps. The samples from the remaining two centres (25% of total participant numbers) were used to validate the accuracy of the algorithms on an independent set of samples, with un-blinding once the Raman spectroscopy test scores were calculated to allow calculation of the accuracy of the validation.

Processing

Raman data collected from the nails of the calibration set were used to create a background correction model based on singular value

decomposition (SVD)-based background removal.^[21,22] Principal component analysis (PCA) was carried out on the non-normalized calibration data, and the first PC score was used to normalize the baseline-corrected data.^[23,24] These models were then applied to the validation data.

The processing methods employed here will now be compared to those used in the study by Mussatto *et al.*, which applied a simple fifth-order polynomial fit to the data. In Fig. 5a of their paper, they present the PC loadings for their dataset. Within that figure, it is clear that PC2 and PC3 exhibit mostly features that are broader than the typical Raman peaks of proteins such as keratin, suggesting that a fifth-order polynomial was not able to reduce the variation in the non-Raman background sufficiently to allow the variation in the Raman signal to dominate the PCA.

The processed data were subjected to further PCA to reduce the data dimensionality followed by applying *t*-tests to the PC scores to identify the most informative PCs. This ensures that the minimal number of variables was submitted to linear discriminant analysis (LDA), reducing the risk of over-fitting. Cross validation within the calibration set provided a model that was then tested on the validation set data. Metrics of classification performance were calculated, but only the area under the curve is reported here. The remaining metrics are reported in a manuscript that considers the clinical implications of the study.^[18]

Figure 1a shows the mean raw signal collected from the human fingernails measured in the study along with the mean raw signal for samples from participants that had sustained a fracture and mean raw signal for samples from participants that had not. Compared to the fracture cases, the nonfracture controls have an elevated peak in the broad non-Raman background at around

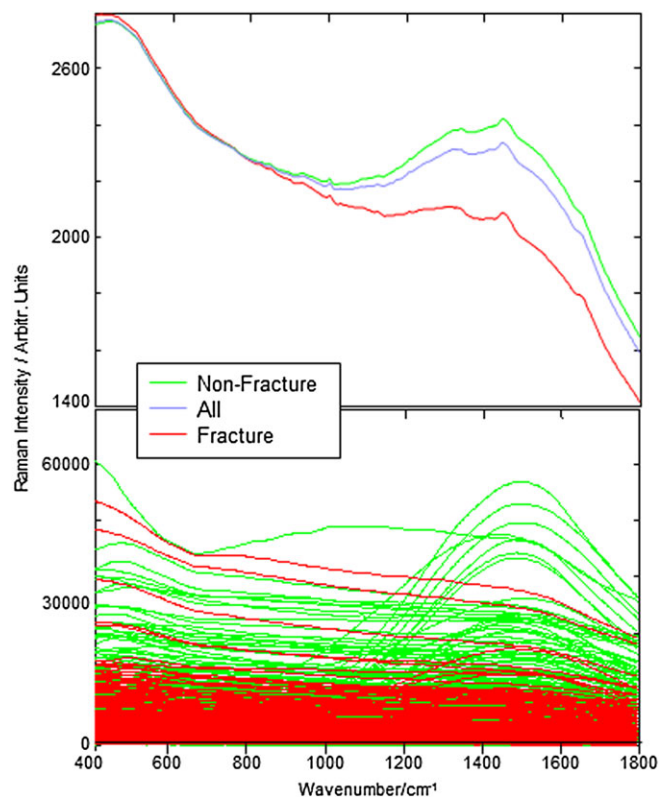


Figure 1. Raw signals collected using a Raman spectrometer on human fingernails. (a) Mean raw signals for nonfracture control, fracture case and all spectra. (b) Individual raw signals for nonfracture control and fracture case samples. [Colour figure can be viewed at wileyonlinelibrary.com]

1450 cm^{-1} , and when the individual raw signals are compared (Fig. 1b), it is clear that the control group does indeed have a preponderance of raw signals exhibiting a strong peak centred around 1450 cm^{-1} , and so for this reason it was decided to also attempt discrimination using the raw signals to determine if this apparent difference was useful for diagnosis. To ensure no bias was introduced due to intensity variations, the discriminatory power of the raw data was tested without normalization, normalization to full area and normalization to the same normalization factor used for the baseline-corrected data. The data were reduced by PCA, *t*-test for significance followed by LDA.

Spectral assignment

Because human nail is >95% keratin, the majority of the Raman signal is constant so, in order to simplify spectroscopic assignment of the spectra prevalent in the cases and controls, partial subtraction spectra were generated by determining the relative scaling for the subtrahend required to reach the point just before the appearance of negative features in the subtraction spectrum. A traditional subtraction spectrum based on equal mean intensity was also generated for reference as this is the more usual format reported. The partial subtraction spectra were then compared to spectra for each amino acid to assess the possibility of each contributing to the spectra. Each peak in the amino acid spectra was assessed for coincidence with features present in the case and control spectra, as illustrated conceptually in Fig. 2. Although this figure shows just three peak comparisons for illustrative purposes, the comparison is carried out for every peak that exists in the reference amino acid spectrum as is presented in the supplementary figures and explained in more detail in Appendix 1. An amino acid peak coincidence is made confidently when the amino acid spectrum exhibits a distinct band that is also observed in the subtraction spectrum, with that peak assigned a tick mark in the figure. An assignment is rejected confidently if the amino acid spectrum exhibits distinct unique bands that are not observed in

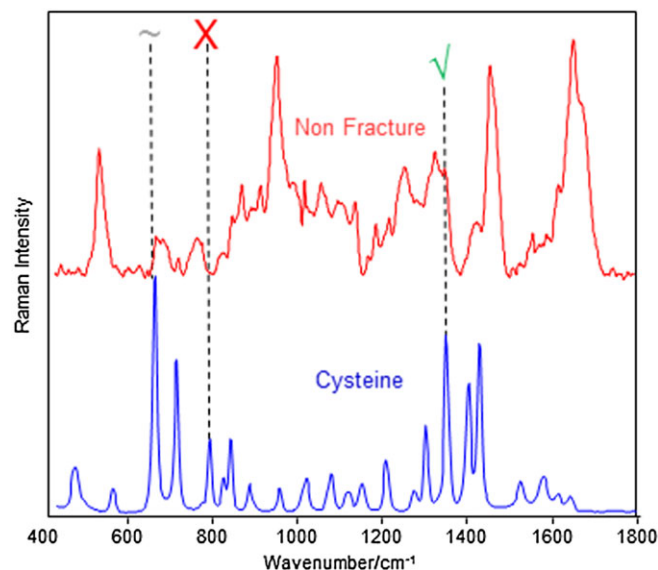


Figure 2. Example of partial subtraction spectra being compared to amino acid spectra (offset for clarity), illustrating amino acid Raman bands with centres that coincide with peak centres (✓), minima (X) and bands which are not definitively either (↔). [Colour figure can be viewed at wileyonlinelibrary.com]

the subtraction spectrum, as indicated by an X in the figure. If a band observed in the amino acid spectrum is similar to, but not exactly matching, a peak in the subtraction spectrum, the peak is labelled as uncertain (indicated by ~ on the figure). The presence of a cross rules out the contribution of that amino acid to the subtraction spectrum, as will a preponderance of uncertain assignments. The comparisons of the subtraction spectra with all the amino acid spectra are made available as supporting information (Supplementary Figs. 1–16).

Results

The raw signals presented in Fig. 1 visually hint that there may be some discriminatory power, with respect to fracture, in the raw (unprocessed) signal, but an LDA model constructed from the raw data was unable to produce a reliable discrimination. The Area Under the Curve for the Receiver Operator Characteristics (AUC) against fracture returned by the unprocessed data was 0.67 ($p = 0.00008$) in calibration, but this dropped to 0.55 ($p = 0.21$) in validation. To rule out bias due to lack of controlling for absolute intensity variation, a model that used normalized but not baseline-corrected data was also tested. When normalized by Raman intensity but without baseline correction, the data gave AUC against fracture of 0.56 ($p = 0.06$) and 0.54 ($p = 0.26$) in calibration and validation, respectively.

The data plotted in Fig. 3, when compared to Fig. 1, show that the removal of the non-Raman background allows for a much more consistent signal, with reduced variability between samples within each group. The data processed as detailed in the methodology section however gave stable models with an AUC against fracture of 0.64 and 0.67 ($p = 0.00009$ and 0.0017) in calibration and validation, respectively.

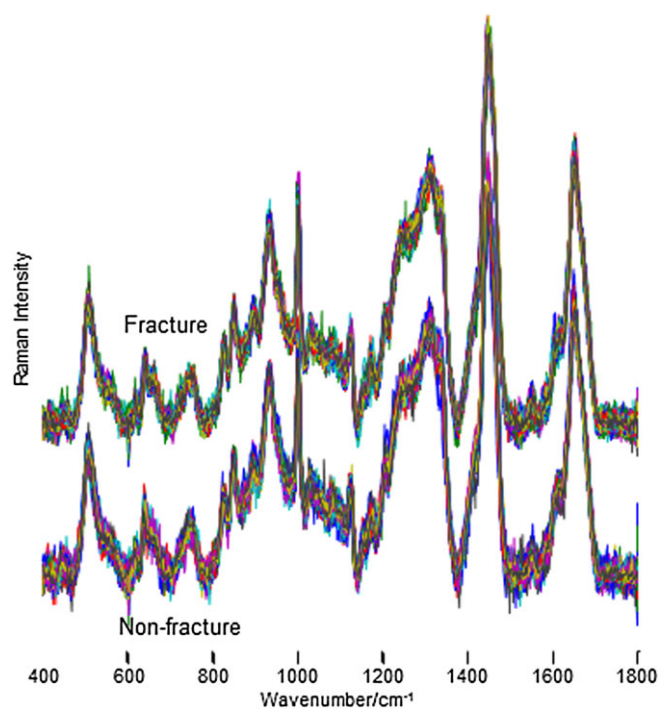


Figure 3. Processed Raman spectra of human fingernails. (a) Fracture cases (offset for clarity). (b) Nonfracture controls. [Colour figure can be viewed at wileyonlinelibrary.com]

The clinical data collected along with the nail samples included a record of osteoporosis diagnosis, allowing comparison between healthy and osteoporotic patients. For the Healthy/pervasive Osteoporotic comparison, the AUC achieved in calibration was 0.76 ($p = 0.005$, $N = 116$). The AUC remained high at 0.78 despite low sample numbers ($p = 0.07$, $N = 23$) in validation. Comparing patients that met the less stringent criteria usually applied clinically of only one site for the osteoporosis diagnosis failed to build a model that performed acceptably in validation [AUC = 0.66 ($p = 0.0002$) and 0.58 ($p = 0.15$), in calibration and validation, respectively].

Interpreting the spectral differences between cases and controls

Figure 1 shows the raw signals that were collected from the fingernails, colour coded according to whether the participant had a fracture or not. There was substantial variation observed (40 PCs exhibited contributions from broad non-Raman contributions), and the complex shape of many of the backgrounds proved too challenging for the traditional approach of estimating the baseline correction on the individual signals (data not shown). Due to the complexity of the variation, SVD-based baseline correction was employed as this allows the analyst to separate out each individual contributor to the background variation and define a specific correction for each source of non-Raman background. Figure 3 shows the processed spectra for the fracture and nonfracture groups. The baseline achieved after correction with the SVD-based approach was consistent and reproducible (the reader is encouraged to compare the spectra in Figs 1 and 3). Out of 633 samples, only one was unable to yield a useable Raman signal after baseline correction as it had such a large non-Raman background it was not possible to record a signal greater than the noise within the accumulation time (noise level is dependent on total signal, so presence of very large non-Raman signals increases the noise level relative to the Raman features).

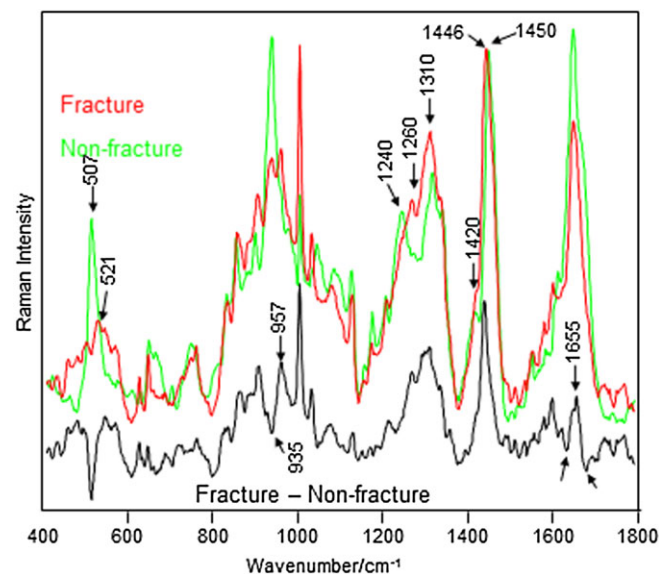


Figure 4. Partial subtractions (scaled so that no negative peaks appear in the subtraction) of the fracture minus nonfracture (midgrey) and the nonfracture (light grey) minus fracture, with peak positions labelled. Also included is the one to one subtraction normalized to total peak area (black). [Colour figure can be viewed at wileyonlinelibrary.com]

Figure 4 compares the partial subtraction average spectra for the case and control spectra for the fracture *versus* nonfracture comparison and indicates the central Raman shift for a number of peaks. Also included is the more traditional difference spectrum between the two, with the spectra normalized to mean intensity before subtraction. In the traditional difference spectrum, the subtraction is case minus control, so features dominant in the cases are positive and peaks dominant in the controls are negative. The prominent peaks in each positive spectrum are labelled for reference. A number of key features are apparent in this figure, and assignments of common bands in proteins are provided in Table 1.^[25–27] In keeping with previous findings,^[7–10] there is a change in the region where the disulphide mode is found, just above 500 cm^{-1} , with the mean nonfracture spectrum exhibiting a more intense feature centred around 507 cm^{-1} , while the mean fracture spectrum shows a broader flatter peak centred around 521 cm^{-1} . Table 2 summarizes the different amino acid residue assignments that could be made against the full spectra. Figures illustrating the comparison between the fracture/nonfracture difference spectra and groups of amino acids are shown in Supplementary Figs 1 to 8.

The spectral assignments for the amino acids fall into categories of types of amino acids. In the nonfracture controls, there is a significant elevation of disulphide bonding (cystine), which contrasts against elevated broken disulphides (cysteine) in the fracture cases. In the fracture cases, there is a significant and consistent elevation of all of the aromatic and aliphatic, acidic and amide amino acids, but no consistent change in the hydroxyl and basic amino acids. A further supporting piece of evidence for elevated aliphatic amino residues in the fracture group is the central wavenumber shift of the scissor mode at 1446 cm^{-1} ; this is characteristic of the aliphatic amino acids, while the typical position for this band in proteins is

1450 cm^{-1} . Only three amino acids appear to contribute significantly more intensity to the nonfracture control group signals, namely cysteine (described above in relation to disulphide bonding), glycine and serine. A number of amino acids also appear in both cases and controls but exhibit slight changes in band positions and relative intensities that indicate that the local conditions of these amino acids are changing indicating structural differences. Tryptophan, methionine and tyrosine all appear to exhibit band changes going from control to case that can be attributed to a decrease in hydrophilicity. There is no evidence to support the presence of proline or hydroxyproline in either group.

In addition to the amino acid composition, the Raman spectrum of proteins also encodes key information regarding the secondary structure of proteins. The amide I region ($1630\text{--}1690\text{ cm}^{-1}$) contains relatively few contributions from amino acid side chains and is much more readily interpreted, but the amide III region ($1220\text{--}1320\text{ cm}^{-1}$) and C–C stretching modes (920 and 1010 cm^{-1}) are included to cross check the assignment. The positions of the peaks in the nonfracture controls are 1635 , 1680 , 1310 , 1240 and 935 cm^{-1} , indicating that these samples exhibit a stronger contribution from alpha helical and beta sheets, while the fracture cases have a stronger contribution from so-called 'random' structure as indicated by increased intensity at 1655 , 1260 and 957 cm^{-1} .^[28]

The partial subtraction spectra for the osteoporotic/healthy comparison are shown in Fig. 5. The partial subtraction for the osteoporotic group shares many features with that of the fracture group including the region from 800 to 1100 cm^{-1} . However, there are notable deviations between these two disease groups, such as in the disulphide region and in the acid/amide region around 1410 cm^{-1} . The control groups also share many features in the $800\text{--}1100\text{ cm}^{-1}$ region and with similar contributions related to alpha helices at 1635 , 1310 (superimposed on a broader decrease) and 935 cm^{-1} . However, the beta-sheet contributions are elevated in the osteoporosis group compared to the healthy, the opposite to the disease/control pattern observed for fracture. The disulphide band also makes a dramatically lower contribution to the healthy group than to the nonfracture group, while the osteoporosis cases exhibit a broad band in this region. Sharp Raman bands indicate a highly co-operative physical structure, while the bands broaden as the physical structure becomes more disordered. The location of the disulphide stretching mode is sensitive to the angles of the neighbouring chemical bonds, so a broader band indicates a greater variety in local conformations.^[29] This infers that while osteoporosis is not associated with a loss of disulphide bonding, it is associated with a loss of systematic, consistent orientation of the proteins adjacent to these bonds.^[30] The band around 1420 cm^{-1} in the nonfracture group is absent from the healthy group but is strong in the osteoporotic patients, a position associated with carboxylic groups typical in acids and amides. None of the acid nor amide amino acids were unambiguously identified in either the healthy or osteoporosis partial subtraction spectrum, suggesting that changes in the environment of the acid and amide groups account for the changes around 1420 cm^{-1} , rather than changes in the proportions of these residues within the proteins. In general, the osteoporosis/healthy comparison exhibited fewer changes that could be matched up to entire amino acid spectra than was the case for the fracture/nonfracture comparison.

The partial subtractions for the control groups (nonfracture and healthy) are more similar (share 62% of intensity) than for the disease groups (fracture and pervasive osteoporosis, which share 51% of intensity). In contrast to the fracture-based comparison,

Table 1. Assignment of common bands in the Raman spectrum of proteins

Band position (cm^{-1})	Assignment
510	Cys–Cys S–S stretch. GGG conformation
525	Cys–Cys S–S stretch. GGT conformation.
642–644	Tyr
661–670	Cys C–S stretch
750–752	Trp
820–830 with 850–860	Tyr
880–884	Trp
920–950	C–C stretch in α helix
960	C–C stretch in random structure
1000	C–C stretch in β sheet (weak + broad)
1003	Phe ring breathing
1032	Phe, Tyr ring bending
1050–1130	C–C, C–N, C–O stretching modes
1225–1235	Amide III in β sheet
1250–1255	Amide III in random
1265	Amide III in globular α helix
1305	Amide III in fibrous α helix
1408–1422	COO^-
1438	COOH
1450	CH_2 scissor (increases with hydrophilic interactions)
1530–1630	Phe, Tyr, His, Trp various ring modes
1645–1658	Amide I in α helix
1660–1665	Amide I in random
1665–1680	Amide I in β sheet

Table 2. Amino acid assignments for partial difference spectra. Figures comparing spectra to individual amino acid spectra are found in supplementary figures

Class	Name	Code	Fracture	Nonfracture	Osteoporotic	Healthy	Side chain structure
No Side Chain	Glycine	Gly	X	√	√	√	-H
Aliphatic	Alanine	Ala	√	X	√	X	-CH ₃
Aliphatic	Valine	Val	√	X	X	X	-CH(CH ₃) ₂
Aliphatic	Leucine	Leu	√	X	X	X	-CH ₂ CH(CH ₃) ₂
Aliphatic	Isoleucine	Ile	√	X	X	X	-CH(CH ₃)CH ₂ CH ₃
Aliphatic	Proline	Pro	X	X	X	X	-(CH ₂) ₃ -(αX)
Aromatic	Phenylalanine	Phe	√	X	√	X	-CH ₂ Ph
Aromatic	Tyrosine	Tyr	√	√	√	√	-CH ₂ Ph-OH
Aromatic	Tryptophan	Trp	√	√(aq)	√	√(aq)	-CH ₂ In
Sulphur	Cysteine	Cys	√	X	X	X	-CH ₂ SH
Sulphur	Cystine	Cys-Cys	X	√	√	√	-CH ₂ S-SCH ₂ -
Sulphur	Methionine	Met	√	√(aq)	X	X	-CH ₂ CH ₂ SCH ₃
Acidic	Aspartic Acid	Asp	√	X	X	X	-CH ₂ COOH
Acidic	Glutamic Acid	Glu	√	X	√	X	-CH ₂ CH ₂ COOH
Amide	Asparagine	Asn	√	X	X	√	-CH ₂ CONH ₂
Amide	Glutamine	Gln	√	X	√	X	-CH ₂ CH ₂ CONH ₂
Basic	Lysine	Lys	X	X	X	X	-(CH ₂) ₄ NH ₂
Basic	Arginine	Arg	X	X	X	X	-(CH ₂) ₃ NHC(=NH)NH ₂
Basic	Histidine	His	X	X	X	X	-CH ₂ Py
Hydroxyl	Serine	Ser	X	√	X	X	-CH ₂ OH
Hydroxyl	Threonine	Thr	X	X	√	X	-CH(CH ₃)OH
Hydroxyl	Hydroxy Proline	HPro	X	X	X	X	-(CH ₂) ₂ CHOH-(αX)

the differences in matched amino acid residue spectra were not as consistent, with the exception of the aromatic amino acid residues, which exhibited very similar patterns. Fewer amino acids fitted the pattern of peaks in the osteoporosis-based partial subtractions, suggesting that the content of fewer amino acid residues are changing in this pathology. Indeed, the overall correlation between the discriminant functions for predicting nonfracture/fracture and for predicting pervasive healthy/osteoporotic status is weak, with

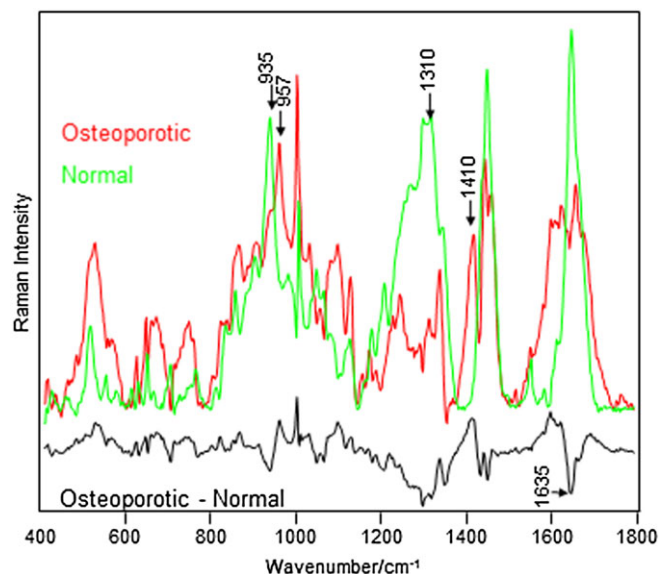


Figure 5. Partial subtractions (scaled so that no negative peaks appear in the subtraction) of the osteoporosis - normal (mid grey) and the normal - osteoporosis (light grey), with peak positions labelled. Also included is the one to one subtraction normalized to total peak area (black). [Colour figure can be viewed at wileyonlinelibrary.com]

an R^2 of 0.107. The correlation between the Raman fracture score and the DXA scan results across all patients was 0.018.

Figure 6 shows the scatter for the fracture and osteoporosis scores with the combinations of fracture status (shade) and osteoporosis status (shape). The extreme samples in the upper left quadrant contain a high proportion of samples that are from nonfractured patients (black) but with mixed osteoporosis status (circle and cross). The lower right quadrant extreme samples are mostly individuals with a healthy osteoporosis status (circle) who sustained fractures (grey). The upper right extreme samples are mostly osteoporotic patients (cross) who have sustained a fracture (grey).

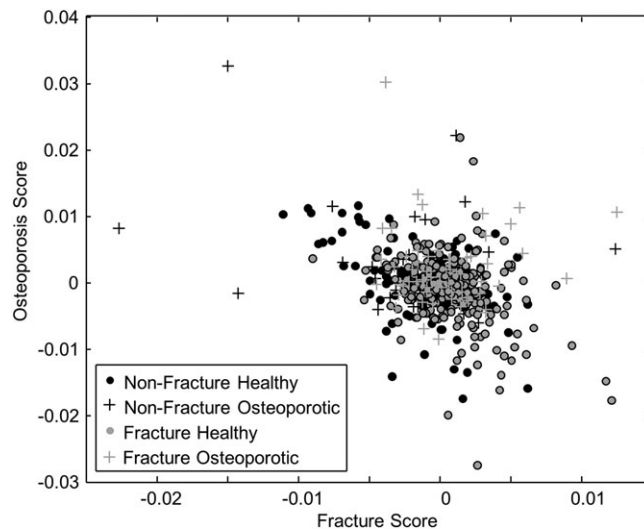


Figure 6. Scatter graph of the fracture score versus the osteoporosis score derived from the Raman spectra of human nails. Shade indicates the fracture status, while shape indicates the osteoporosis status.

Discussion

Amino acid identification

The amino acids that appear in the fracture spectrum fall into five groups: aliphatic, aromatic, acidic, amide and sulphurous (Table 2). No evidence for significant contributions from basic or hydroxyl amino acids could be found, and there was no evidence for disulphide bonds in the fracture subtraction spectrum compared to a distinct contribution in the nonfracture group. Although the nonfracture subtraction spectrum also contains contributions from all the aromatic amino acids, these appear at lower concentrations and with some perturbations indicating a change to the local environment. For example, the tyrosine doublet near 830/850 cm^{-1} is two wavenumbers lower for the nonfracture controls with a narrower bandwidth and a decreased relative intensity at the 850 cm^{-1} mode. This suggests that tyrosine in the nonfracture group is slightly less exposed and more consistently oriented than in the fracture group. The nonfracture group also contains acidic amino acid contributions evidenced by strong bands at 1042, 1420 and 1745 cm^{-1} , with glutamic acid providing a better match than aspartic acid. Changes in the ionization of the acid residues (as evidenced by the 1420 cm^{-1} band) appear weak in the nonfracture *versus* fracture comparison (the peak centre moves but intensity remains constant), but a dramatic difference is observed in the healthy *versus* osteoporotic group (where the band occurs at 1410 cm^{-1}). The osteoporotic group shows a strong peak associated with free acid, suggesting that systemic factors affecting the ionization of acid residues and their binding to bone mineral are also affecting the ionization of the acid residues in nail keratin. There are possible contributions from amide and hydroxyl, but most aliphatic amino acids can be ruled out except glycine and leucine.

In addition to changes in the individual amino acid residues, the Raman spectra suggest significant changes within the secondary and quaternary structure of the nail keratin between the fracture and nonfracture groups. The secondary structure shows a slight change from a more ordered (alpha helices and beta sheets) toward a less systematically ordered structure moving from nonfracture to fracture. These changes would be expected to induce subtle changes in the structural properties of the keratin as was found previously.^[7,10,31] The reduction in disulphide bonding would indicate a reduction in quaternary structure, with fewer cross-links between neighbouring chains of keratin, which would be expected to further reduce the structural integrity of the nail keratin.

The gold standard method for assessment bone health is bone densitometry using DXA, which measures the density of mineral within the bone. Low BMD typically accounts for only around 30–40% of risk of fragility fracture (in the study reported here the proportion was 25%), and it is accepted that other aspects of bone structure must be associated with the remaining fracture risk. Bone quality refers in part to the organic matrix of bone but also describes a set of characteristics that influence strength such as architecture, re-modelling and damage accumulation.^[32] Changes in the organic matrix or in the collagen molecule alone have been observed in osteoporosis and can affect bone strength.^[33] Biochemical markers of bone remodelling are used in clinical practice to assess bone quality, and they have been reported to predict bone loss^[34] and future fracture risk.^[35]

The very low level of correlation between the subtraction spectra for the fracture/nonfracture and for the osteoporosis/healthy

situations suggests that the markers of fracture risk that are being detected in the Raman spectra of human finger nail are not strongly related to BMD but rather are measuring a surrogate marker of a different aspect of bone quality, such as changes in the organic matrix of the bone.

Several of the spectral changes measured in the Raman spectra between nonfracture and fracture groups can be attributed to changes in the order of the proteins, going from highly structured alpha helical structure with ample intra-chain disulphide bonding to a state of less ordered 'random' secondary structure and a breakdown in intra-chain disulphide bonding. We propose that the Raman spectra of human fingernails present a surrogate marker of bone protein structure status. If the bone collagens were to be disordered in the same way as the nail keratin, this would be expected to reduce the co-operativity of the elastic collagen scaffold, reducing the bone's ability to recoil from an impact.

The spectral changes associated with the distinction between healthy and pervasive osteoporosis suggest that the proteins do not become random as in the fracture situation but do show a transition from alpha helices to another ordered (and generally more stable) form, beta sheets. This change of folding alters the orientation of the amino acid residues and therefore what groups are exposed to potential phosphate nucleation. The spectra also suggest that significantly more of the acid residues are ionized in the pervasive osteoporosis group. Acid groups are critical for forming a link between bone mineral and the bone collagen scaffold,^[36] and any changes that would impact the ionization of these groups could impact the ability of phosphates to bind to these groups and therefore form a nucleus for bone mineral crystal formation. These protein-based changes are an indirect effect leading to a magnified impact on the decrease in bone mineral binding. Such an amplification effect means that the protein changes associated with osteoporosis would be more challenging to detect. Further work is ongoing to assess the validity of this hypothesis.

The scatter of the data in Fig. 6 suggests that there may be some separation between osteoporotic patients who do and who do not sustain a fracture. The number of osteoporosis patients within this study is insufficient to provide statistical power to evaluate the robustness of this apparent effect. Further investigation in a larger population of osteoporotic patients would be required to more completely evaluate the ability to identify those osteoporotic patients who are at most risk of fracture.

Spectral processing

The raw data presented in Fig. 1 visually suggest that there may be differences between the raw data for the case and controls, and in fact a statistically significant AUC was obtained from a model calibrated using the unprocessed data. However, this model was unable to sustain validity in a validation set. This type of behaviour indicates that while there are some differences in the non-Raman background between the cases and controls, the variation in the background is not sufficiently reliable to build a predictive model.

Mussatto *et al.*^[17] assessed the relationship between the Raman spectra of human nails and osteoporosis diagnosis but were unable to find significance. Figure 1 of this current manuscript shows that the non-Raman background, using an excitation wavelength of 785 nm (Mussatto *et al.* used 830 nm which will change the background profiles encountered), is extremely variable and requires a more adaptive approach to baseline correction than the more traditional type of approach used by Mussatto *et al.* Figure 3 in this

current manuscript shows how consistently the SVD-based approach is able to standardized the baseline of the Raman signals. The difference in stability between the models built from the processed and unprocessed data demonstrates that it is critically important to eliminate as much of the variation in the non-Raman background as possible.

This manuscript confirms that a reliable difference can only be detected between the most extreme cases on the osteoporotic scale, and even then the result did not quite reach significance on validation (although this could be attributed to the very low sample numbers that met the criteria for osteoporosis at every site). Conversely, the discrimination between nonfracture control and fracture case was a more reliable model

Conclusions

This study demonstrates that the Raman spectra of human fingernail can offer a window into a subject's bone health. This is achieved by probing the protein composition and structure of human fingernail, as measured by Raman. The study also demonstrated that the facets of bone health that the Raman spectra of nails are best able to detect are largely unrelated to the pathology of osteoporosis, which is indicated by loss of bone mineral. Consequently, the presented data suggest that while the Raman spectra of human nail are affected by factors affecting BMD, the effect size is not as large as that encountered against fracture risk.

For the fracture group compared to the nonfracture controls, the data suggest that there are significant structural defects accumulating in the keratin from the nails collected from the fracture group. Alongside these structural defects, there appear to be differences in the amino acid composition of the two groups, with entire classes of amino acid residues being elevated in the fracture group.

The data present above suggest that the development of osteoporosis is associated with different protein changes than are observed with a general increased risk of fragility fracture. The changes associated with osteoporosis appear to be more structural than compositional (fewer amino acids can be matched to the subtraction spectra) and may reflect that the main change in osteoporosis is the ability of the proteins to interact with bone mineral. In addition, the changes to the ionization of the acid groups in bone collagen play an important role in the nucleation of phosphate crystallization, the process whereby bone mineral is bound to the collagen scaffold.

Our hypothesis for how the changes in keratin correlate with changes in fracture risk is that systemic conditions in the body could have a mediating influence on the growth and maintenance of structural proteins throughout the body. Further work is needed to investigate if similar changes can be observed in osteoporotic and healthy bone collagens.

Dual energy X-ray absorptiometry is a well-established method for assessing bone health and, with good reason as a positive diagnosis of osteoporosis, is associated with an elevated risk of fracture. However, DXA is limited to only being able to detect the risk of fracture for a subset of patients, and typically 60–70% of fragility fracture patients will not meet the criteria for osteoporosis. Raman measurements of the human fingernail, however, correlate with a different dimension of fracture risk, demonstrating a potential role in fracture risk assessment, that of identifying patients who are at risk of fracture for reasons other than low BMD.

Acknowledgment

This work was funded by Crescent Diagnostics Ltd and Crescent Ops Ltd.

Author disclosures

Dr. Renwick Beattie and Dr Clare Caraher were formerly employees and currently consultants to Crescent Ops Ltd, a company which owns intellectual property rights on the relationship between Raman spectroscopy, nail structure and fracture risk. R.B. is also a shareholder in Crescent Ops Ltd. Professor Mark Towler is both a shareholder in, and a consultant to, Crescent Ops Ltd. Dr. Niamh Cummins and Ms. Olive O'Driscoll have served as consultants for Crescent Ops Ltd. Prof. Eastell consults for Lilly, Amgen, Merck and Novartis.

Reference

- [1] J. Kanis, Assessment of osteoporosis at the primary health care level, *World Health Organ.* **2007**.
- [2] O. Johnell, J. A. Kanis, *Osteoporos. Int.* **2004**, *15*, 897.
- [3] J. A. Kanis, O. Johnell, C. De Laet, B. Jonsson, A. Oden, A. K. Ogelsby, *J. Bone Miner. Res.* **2002**, *17*, 1237.
- [4] S. Boonen, P. Autier, M. Barette, D. Vanderschueren, P. Lips, P. Haentjens, *Osteoporos. Int.* **2004**, *15*, 87.
- [5] J. A. Kanis, E. V. McCloskey, H. Johansson, A. Oden, L. J. Melton 3rd, N. Khaltaev, *Bone* **2008**, *42*, 467.
- [6] D. Lyons, *Fingernails in Osteoporosis*, **2002**.
- [7] I. Pillay, D. Lyons, M. J. German, N. S. Lawson, H. M. Pollock, J. Saunders, S. Chowdhury, P. Moran, M. R. Towler, *J Womens Health (Larchmt)* **2005**, *14*, 339.
- [8] M. R. Towler, A. Wren, N. Rushe, J. Saunders, N. M. Cummins, P. M. Jakeman, *J. Mater. Sci. Mater. Med.* **2007**, *18*, 759.
- [9] N. M. Cummins, J. C. C. Day, A. Wren, P. Carroll, N. Murphy, P. M. Jakeman, M. R. Towler, *Spectroscopy* **2010**, *24*, 517.
- [10] P. Moran, M. R. Towler, S. Chowdhury, J. Saunders, M. J. German, N. S. Lawson, H. M. Pollock, I. Pillay, D. Lyons, *J. Mater. Sci. Mater. Med.* **2007**, *18*, 969.
- [11] P. Matousek, E. R. C. Draper, A. E. Goodship, I. P. Clark, K. L. Ronayne, A. W. Parker, *In Vivo. Appl. Spectrosc.* **2006**, *60*, 758.
- [12] S. Wessel, M. Gniadecka, G. B. E. Jemec, H. C. Wulf, *Biochim. Biophys. Acta-Protein Struct. Mol. Enzymol.* **1999**, *1433*, 210.
- [13] E. Widjaja, R. K. H. Seah, *Appl. Spectrosc.* **2006**, *60*, 343.
- [14] D. L. A. De Faria, M. A. de Souza, *J. Raman Spectrosc.* **1999**, *30*, 169.
- [15] W. Akhtar, H. G. M. Edwards, *Spectrochim. Acta Part A Mol. Biomol. Spectrosc.* **1997**, *53*, 81.
- [16] E. Widjaja, M. Garland, *Talanta* **2010**, *80*, 1665.
- [17] J. C. Mussatto, M. C. Perez, R. A. de Souza, M. T. T. Pacheco, R. A. Zangaro, L. Silveira Jr, *Lasers Med. Sci.* **2015**, *30*, 287.
- [18] J. R. Beattie, N. Cummins, C. Caraher, O. O'Driscoll, A. Bansal, R. Eastell, S. Ralston, M. Stone, G. Pearson, M. Towler, *Clin. Med. Insights (Arthritis Musculoskelet. Disord.)* **2016**, *9*, 109.
- [19] World Medical Association, World Medical Association Declaration of Helsinki: ethical principles for medical research involving human subjects, *JAMA* **2013**, *310*, 2191.
- [20] WHO, Assessment of fracture risk and its application to screening for postmenopausal osteoporosis: report of a WHO study group [meeting held in Rome from 22 to 25 June 1992], *Tech. Rep. Ser.* **1994**, *843*, 8.
- [21] J. R. Beattie, *J. Raman Spectrosc.* **2011**, *42*, 1419.
- [22] J. R. Beattie, J. J. McGarvey, *J. Raman Spectrosc.* **2013**, *44*, 329.
- [23] J. Palacký, P. Mojžeš, J. Bok, *J. Raman Spectrosc.* **2011**, *42*, 1528.
- [24] J. R. Beattie, J. V. Glenn, M. E. Boulton, A. W. Stitt, J. J. McGarvey, *J. Raman Spectrosc.* **2009**, *40*, 429.
- [25] A. T. Tu, *Raman Spectroscopy in Biology: Principles and Applications*, John Wiley and Sons, New York, **1982**.
- [26] T. Spiro, *Biological applications of Raman spectroscopy*, John Wiley and Sons, New York, **1986**.
- [27] J. Beattie, S. Bell, C. Borggaard, B. Moss, *Meat Sci.* **2008**, *80*, 1205.

- [28] J. R. Beattie, S. Finnegan, R. W. Hamilton, M. Ali, C. F. Inglehearn, A. W. Stitt, J. J. McGarvey, P. M. Hocking, W. J. Curry, *Investig. Ophthalmol. Vis. Sci.* **2012**, *53*, 413.
- [29] A. Weselucha-Birczyńska, M. Kozicki, J. Czepiel, M. Birczyńska, *Analyst* **2013**, *138*, 7157.
- [30] K. Nakamura, S. Era, Y. Ozaki, M. Sogami, T. Hayashi, M. Murakami, *FEBS Lett.* **1997**, *417*, 375.
- [31] G. Pandey, T. Nakamura, R. P. Singh, in Proceedings of the XIth International Congress and Exposition, **2008**.
- [32] National Institutes of Health, Osteoporosis Prevention, Diagnosis, and Therapy, *NIH Consensus Statement Online* **2000**, *17*, 1–36.
- [33] A. J. Bailey, L. Knott, *Exp. Gerontol.* **1999**, *34*, 337.
- [34] C. H. Chesnut, N. H. Bell, G. S. Clark, B. L. Drinkwater, S. C. English, C. C. Johnson Jr, M. Notelovitz, C. Rosen, D. F. Cain, K.A. Flessland, N. J. Mallinak, *Am. J. Med.* **1997**, *102*, 29.
- [35] P. Garnero, E. Hausherr, M. C. Chapuy, C. Marcelli, H. Grandjean, C. Muller, C. Cormier, G. Bréart, P. J. Meunier, P. D. Delmas, *J. Bone Miner. Res.* **1996**, *11*, 1531.
- [36] O. Karaman, A. Kumar, S. Moeinzadeh, X. He, T. Cui, E. Jabbari, *J. Tissue Eng. Regen. Med.* **2013**. DOI:10.1002/term.1775.

Supporting information

Additional Supporting Information may be found online in the supporting information tab for this article.

Appendix 1: Amino acid assignments

Amino acid spectra were recorded at 785 nm on Jobin Yvon LabRamHR800. The spectra were overlaid with the partial

difference spectra for the fracture cases and the nonfracture controls in LabSpec v5 (Jobin Yvon Horiba) and copied into PowerPoint. The alignment of the amino acid peaks with the difference spectra was checked using the vertical ruler in LabSpec, and the proximity of a match was indicated in the PowerPoint slide, with these figures presented in Supplementary Figs 1–6. A green tick indicates a strong overlap between the presence of a peak in the amino acid reference spectrum and a peak maximum in the partial subtraction spectrum. A grey ~ was used to indicate a peak in the amino acid reference spectrum that was close to a feature in the difference spectrum and cannot be definitively stated to be the same feature but may be slightly shifted. A red X was used to indicate peaks in the amino acid reference spectrum that could not reasonably be matched with any features in the difference spectrum.

Where groups of peaks overlapped, there is an elevation above the baseline at the minima between the peaks. If a peak in the amino acid spectrum corresponded to a local minima that was elevated in this way, it gives a red X because one would not expect a local minima to coincide with a significant peak. A preponderance of red X or a combination of red X and grey ~ can be used to confidently rule out an assignment. If most marks are green ticks, then any discrepancies are checked against the literature to determine if there are any factors that may reasonably have changed a peak's appearance. If that same factor affects other bands in the amino acid, the trace of these changes should be evident in other bands affected by it.